

## Article

# Conventional and Switched Capacitor Boost Converters for Solar PV Integration: Dynamic MPPT Enhancement and Performance Evaluation

Mansour Hawsawi <sup>1,\*</sup>, Hanan Mikhael D. Habbi <sup>2</sup>, Edrees Alhawsawi <sup>1,3</sup>, Mohammed Yahya <sup>1</sup>  
and Mohamed A. Zohdy <sup>1</sup>

- <sup>1</sup> Department of Electrical and Computer Engineering, Oakland University, Rochester, MI 48309, USA; yahya@oakland.edu (M.Y.)  
<sup>2</sup> Department of Electrical Engineering, University of Baghdad, Baghdad 10071, Iraq  
<sup>3</sup> Department of Electrical and Computer Engineering, College of Engineering, Effat University, Jeddah 21478, Saudi Arabia  
\* Correspondence: hawsawi@oakland.edu; Tel.: +1-229-443-5858

**Abstract:** This paper designs two DC-DC converter configurations integrated with solar PV renewable energy resource. Its focuses on comparing two converter topologies: the conventional boost converter and the switched capacitor boost converter. The Perturb and Observe (P&O), Incremental Conductance (INC), Genetic Algorithm (GA), and Particle Swarm Optimization (PSO) algorithms are employed to dynamically enhance the Maximum Power Point Tracking (MPPT) performance for both converters. The simulation results demonstrate that both converter topologies, when integrated with appropriate MPPT algorithms, can effectively harvest maximum power from the solar PV. However, the switched capacitor topology converter exhibits advantages in terms of current capabilities and voltage performance. In addition, combining the switched capacitor boost converter with the GA-MPPT algorithm improved the output voltage profile. The switched capacitor topology demonstrates distinct advantages by exhibiting enhanced current control, enabling improved handling of dynamic load changes and varying irradiance conditions. It shows voltage regulation, resulting in reduced output voltage fluctuations and enhanced stability, thereby optimizing energy extraction. The GA-MPPT simulation demonstrates a substantial increase in maximized output current for the switched capacitor boost configuration (70 A) when compared to the conventional type (10 A). The validation and implementation of the system models are carried out using MATLAB/Simulink.

**Keywords:** conventional boost converter; switched capacitor boost converter; PV solar; MPPT; P&O; INC; PSO; GA



**Citation:** Hawsawi, M.; Habbi, H.M.D.; Alhawsawi, E.; Yahya, M.; Zohdy, M.A. Conventional and Switched Capacitor Boost Converters for Solar PV Integration: Dynamic MPPT Enhancement and Performance Evaluation. *Designs* **2023**, *7*, 114. <https://doi.org/10.3390/designs7050114>

Academic Editors: Mohsin Jamil, Yuanmao Ye and Tomasz Pajchrowski

Received: 8 August 2023  
Revised: 12 September 2023  
Accepted: 15 September 2023  
Published: 29 September 2023



**Copyright:** © 2023 by the authors. Licensee MDPI, Basel, Switzerland. This article is an open access article distributed under the terms and conditions of the Creative Commons Attribution (CC BY) license (<https://creativecommons.org/licenses/by/4.0/>).

## 1. Introduction

DC-DC converters are of immense importance in residential, commercial, and industrial applications. They play a vital role in voltage conversion, allowing seamless integration of devices operating on different voltage levels [1,2]. By efficiently stepping up or stepping down voltages, DC-DC converters optimize power supply efficiency and minimize energy losses during transmission and distribution. They are essential components in renewable energy systems, facilitating energy storage and conversion from sources including solar and wind power [3–5]. DC-DC converters enable efficient power transfer between the battery pack and various components, enhancing overall performance in electric vehicles [6]. In industrial settings, they ensure stable power supply, support automation and data centers, and contribute to power quality and stability [7]. Additionally, DC-DC converters enable the miniaturization and portability of electronic devices while maintaining reliable power supply [8]. Their versatile functionality and efficiency make them indispensable in modern electrical systems, driving progress and effective energy utilization.

Switched-Capacitor (SC) converters, a specialized category of Direct Current to Direct Current (DC-DC) converters, are devised based on principles of charge conservation and have the ability to function utilizing capacitors and switches [9,10]. The core mechanism of these devices operates in a cyclic fashion, consisting of the drawing of charge from the input voltage to the subsequent charging of a capacitor, and its eventual discharge to the output. This cycle accomplishes a conversion from one direct current level to another, enabling a seamless power transfer from the source to the destination [11,12]. SC converters stand apart from inductive converters in their intrinsic operation without the need for inductors [13].

Switched-capacitor converter topology provides a deeper insight into the intricate design of these devices. It refers to the specific configuration and connection of capacitors and switches in an SC converter, which can be adjusted and modified according to output requirements and efficiency goal. The key topologies that are most prevalently used in the industry include series, parallel, ladder, and Fibonacci configurations [14]. Furthermore, the Boost Converter, a variant of the Switched-Mode Power Supply (SMPS), embodies a design that employs a transistor and an inductor for the transfer of energy from the input to the output. This device plays a significant role in amplifying or “boosting” input voltages in order to attain higher output voltages, making it an essential tool in the field of power electronics [15,16].

In the context of the operational mechanism of DC-DC converters, there are two key phases: the “ON” phase and the “OFF” phase. The “ON” phase is characterized by the storage of energy in the inductor while the transistor is activated, while during the “OFF” phase, the energy stored is redirected to the load. To maintain control over the output voltage, the duty cycle is responsible for managing the ratio of “ON” and “OFF” times. Given these characteristics, Boost Converters have found extensive application in various fields including electric vehicles, renewable energy systems, and power factor correction [17–21]. The boost converter serves as a step-up DC to DC converter that effectively converts an input voltage into a higher output voltage. This is accomplished by the storage of energy in an inductor and then delivering it to the load via a capacitor.

Recent trends and advancements in boost converter technology revolve around the enhancement of efficiency, downsizing of the devices, and addressing the issues linked to electromagnetic interference (EMI). Some of these advancements include the introduction of advanced control strategies and the incorporation of GaN (Gallium Nitride) devices in the design of the boost converter, contributing significantly to improving efficiency and reducing size [22].

Murtaza et al. [23] introduced an approach to enhance MPPT in PV arrays by employing a modified boost converter and a sliding mode control (SMC) voltage regulator. A series capacitor-based boost converter is introduced, eliminating the need for a parallel LC in circuit. It demonstrates enhanced high-frequency operation and voltage regulation for SMC. The integration of a series capacitor introduces specific benefits that enhance the converter’s performance and efficiency [24].

Fibonacci Switched Capacitor (SC) DC-DC Converters employ an innovative combination of switches and capacitors, making them distinct in the scope of power electronics [25–27]. This unique design facilitates a wide spectrum of step-up or step-down voltage conversion ratios, rendering them adaptable for various power supply requirements. They achieve high precision voltage levels due to their design and operation, providing flexible solutions for various power supply demands. On the other hand, the k-Fibonacci Switched-Capacitor (SC) DC-DC converter design presents some limitations despite the advantages it offers. The inherent complexity in the design and operation of the k-Fibonacci SC DC-DC converter may pose challenges in manufacturing, maintenance, and error detection. In addition, the practical applicability of this technology could be constrained by specific application requirements and the necessity for rigorous real-world testing and validation, potentially leading to additional cost and time expenditures [28]. As the field of power electronics continues to evolve, new approaches and designs are constantly being explored

and tested [29]. However, there remains a significant challenge in balancing the need for efficiency, compactness, and high performance in various applications. SC converters and boost converters have shown promising results in meeting these demands, but continuous innovation and development are essential to fully harness their potential. The ongoing research and advancements in these areas signify a promising future for DC-DC converters, with much potential still to be unlocked. As the push for renewable energy continues, the integration of SC converters, boost converters, and the likes of the Fibonacci SC DC-DC converter with renewable energy sources such as solar and wind power can offer compelling energy solutions. Integrated with renewable energy sources, these converters can aid in efficient power conditioning and help reduce energy loss. They could also aid in managing the intermittent and variable power output that is characteristic of many renewable sources, thus making such sources more reliable and effective.

Various topologies, such as series, parallel, ladder, and Fibonacci configurations, can be employed in SC converters to optimize output requirements and efficiency goals. Boost converters are widely used in applications such as electric vehicles, renewable energy systems, and power factor correction. Advancements in boost converter technology aim to enhance efficiency, reduce size, and address electromagnetic interference issues. Fibonacci SC DC-DC converters offer unique combinations of switches and capacitors, allowing for a wide range of voltage conversion ratios and precise voltage levels.

The three-level resonant switched capacitor boost converter combines switched capacitor and resonant converter techniques, resulting in improved efficiency, high voltage gain, and reduced component stress [12]. By achieving zero-voltage switching or zero-current switching conditions, the converter reduces switching losses and dissipates less power, leading to enhanced energy conversion efficiency. Additionally, its ability to efficiently step-up voltage makes it suitable for applications requiring high output voltages. The converter's advantages make it particularly relevant for renewable energy systems, such as solar photovoltaic systems, where it can maximize power extraction from low-voltage sources and seamlessly integrate renewable energy into the grid. However, this converter's design complexity, control, and synchronization aspects, limited current handling, voltage stress on capacitors, and potential efficiency trade-offs are important considerations. These drawbacks can affect the practical implementation, performance, and cost-effectiveness of the converter. Proper evaluation of these limitations and the application-specific requirements is necessary to determine the feasibility and suitability of utilizing the optimization techniques can be employed to address these drawbacks and enhance the converter's performance.

Moreover, optimization algorithms and machine learning have significant potential for optimizing the design and operation of DC-DC converters [30–33]. These advanced techniques can be utilized to enhance converter efficiency, preempt, and prevent potential failures, and manage power usage more effectively. The application of AI in the realm of power electronics is a promising area of research and holds immense potential for future developments.

In [34], the authors combined a PI controller and a genetic algorithm of the boost converter to provide a comprehensive approach to assess and enhance wind turbine performance in achieving higher power generation, better control, increased efficiency, or other relevant performance metrics. A hybrid maximum power point tracking (MPPT) method for PV systems under partial shading conditions was utilized. Particle Swarm Optimization (PSO) and Differential Evolution (DE) is proposed in [35]. The bat algorithm (BA) is utilized in [36].

Diverse SC converter configurations offer adaptability, while advancements in boost converters address efficiency and size concerns. The three-level resonant switched capacitor boost converter, with its efficiency gains and applicability in renewable energy situations, illustrates progress, and emerging optimization algorithms, such as genetic algorithms, and AI hold promise for refining performance across various applications.

The conventional MPPT methods face challenges in tracking the global peak and achieving fast maximum power point (MPP) attainment [37]. To address these issues, the proposed method offers a simple and rapid algorithm suitable for renewable energy applications.

This paper proposes two DC-DC boost converter configurations, the conventional and the switched capacitor integrated, along with various MPPT algorithms. The comparison and evaluation of these boost converters, combined with different MPPT algorithms, aid in selecting the most appropriate configuration and algorithm based on renewable energy systems. It contributes to advancing efficient energy harvesting from renewable resources. The proposed MPPT methods, which are PSO, GA, P&O, and INC, demonstrate accurate tracking of maximum power and faster MPP attainment; in addition, its simplicity and the rapid execution of the algorithm further enhance its practicality for solar PV systems. Overall, the simulation results presented in this paper have considerable implications of MPPT techniques in PV systems. Furthermore, the proposed boost configuration provides valuable guidance for system designers aiming to optimize energy harvesting efficiency.

## 2. Materials and Methods

### 2.1. Switched Capacitor Boost Converter Based on Fibonacci

Fibonacci Sequence Switched Capacitor converter (FSSC). Figure 1 displays the schematic diagram of a Fibonacci sequence SC converter. It entails 10 switches (transistor, 3 capacitors, and output capacitors). Switches are used to turn ON and turn OFF the converter that functions in several switching states with suitable gains [38]. The converter was operated by using the rule of Table 1. The odd number switches are operational in stage 1, and the even number switches are operational in stage 2. In this converter the voltage gain is increased gradually in each stage based on Fibonacci sequence number (1, 1, 2, 3, 5, 8, 13, 21, ...), the value of voltage in the capacitor becomes  $V_{in}$ ,  $2V_{in}$ ,  $3V_{in}$  and  $5V_{in}$ .

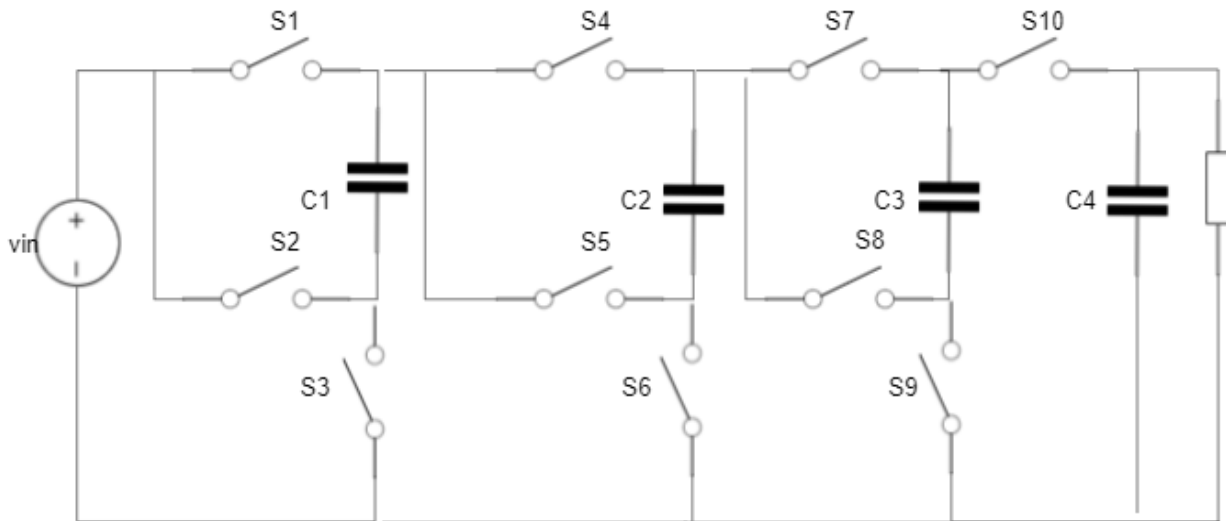


Figure 1. Schematic diagram of 3rd stage Fibonacci sequence SCBC.

Table 1. Switching rule of conventional Fibonacci sequence SC converter.

Step	Switches to Turn ON	Switches to Turn OFF
Mode 1	S1, S3, S5, S7, S9	S2, S4, S6, S8, S10
Mode 2	S2, S4, S6, S8, S10	S1, S3, S5, S7, S9

The output voltage is [1]

$$V_{out} = V_{in} + V_{in} \times \sum_{n=1}^K F_n \tag{1}$$

where:  $F_n$ : the Fibonacci sequence number  $F_1 = 1, F_2 = 1, \text{ for } n \geq 3; F_n = F_{n-1} + F_{n-2}$ ,  $K$ : the stage's number

Figure 2 shows the Fibonacci sequence converter mode 1. In this mode the converter operates 5 transistor switches that charge the C3 up to 3 times the input voltage. Figure 3 shows the Fibonacci sequence converter mode 2. In this mode, the converter operates 5 transistor switches that charge the C3 up to 5 times the input voltage and discharge the capacitor's energy into the output. By applying Kirchoff's voltage and current laws (KCL, KVL) in each loop for mode 1 and 2 for Figures 2 and 3, the state is calculated by:

$$V_{in} = Z1 \times (I1 - I2) \tag{2}$$

$$= Z1 \times (I2 - I1) + Z2 \times I2 + Z3 \times I3 \tag{3}$$

$$V_{out} = I3 * ZL \tag{4}$$

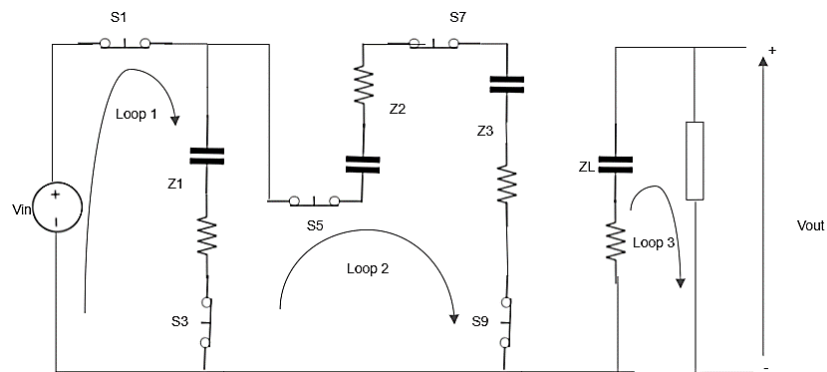


Figure 2. Mode 1 of Fibonacci SCBC.

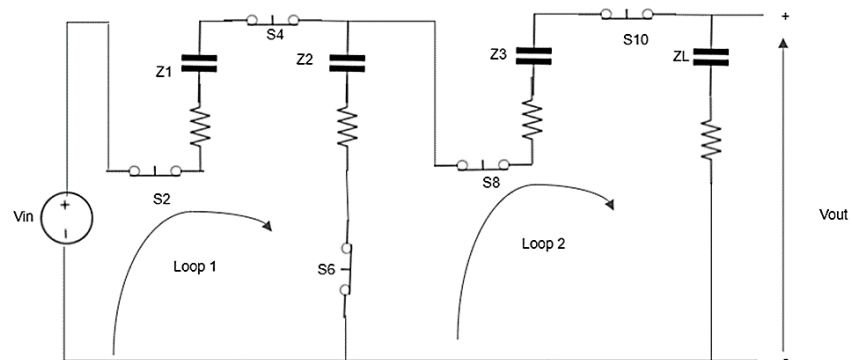


Figure 3. Mode 2 of Fibonacci SCBC.

The impedances  $Z1, Z2,$  and  $Z3$  are the series combination of  $R$  and  $C$ . the state space representation for Mode 1.

$$\begin{bmatrix} V_{in} \\ 0 \\ V_{out} \end{bmatrix} = \begin{bmatrix} Z1 & -Z1 & 0 \\ -Z1 & Z1 + Z2 + Z3 & 0 \\ 0 & 0 & ZL \end{bmatrix} \begin{bmatrix} I1 \\ I2 \\ I3 \end{bmatrix} \tag{5}$$

$$V_{in} = I1 \times (Z1 + Z2) - I2 \times Z3 \tag{6}$$

$$V_{out} = I3 \times ZL + (Z2 + Z3) \times I2 - Z2 \times I1 \tag{7}$$

The state space representation for Mode 2.

$$\begin{bmatrix} V_{in} \\ V_{out} \end{bmatrix} = \begin{bmatrix} Z1 + Z2 & -Z2 & 0 \\ -Z2 & Z2 + Z3 & ZL \end{bmatrix} \begin{bmatrix} I1 \\ I2 \\ I3 \end{bmatrix} \tag{8}$$

2.2. Conventional Boost Converter

Figure 4 displays the conventional boost converter. The output voltage is greater than the input voltage. S1 was used as turn ON and turn OFF to achieve the desire output voltage. The function of the boost DC-DC converter can be split into two states: Mode 1 and Mode 2. In mode 1, S1 is turn ON, the input current rises linearly and flows through the inductor L1, S1, and diode D1 is on reverse bias acting as open switch [10,39]. In mode 2, S2 is turn OFF, the stored current in the inductor flows through the C1, resistive load and D1 is on forward bias acting as closed switch. Figure 5a,b illustrates the two modes of circuit’s operation.

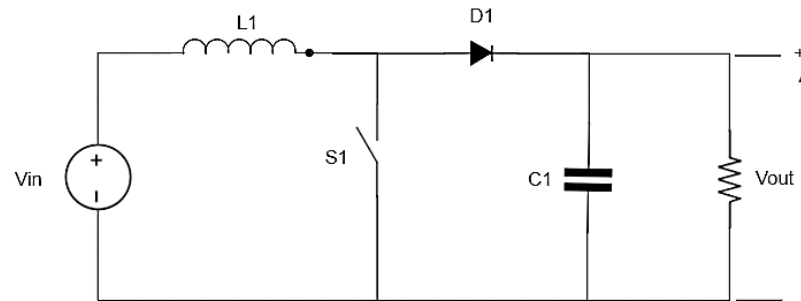
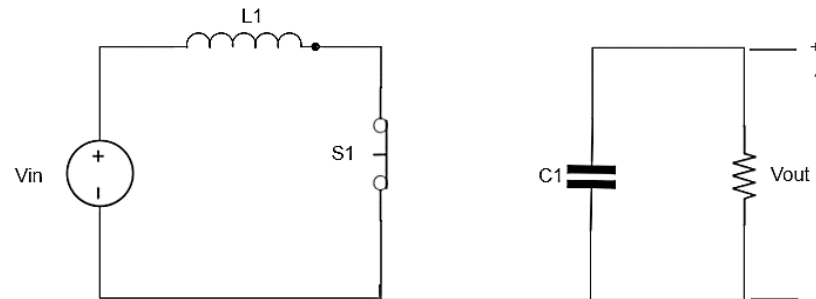
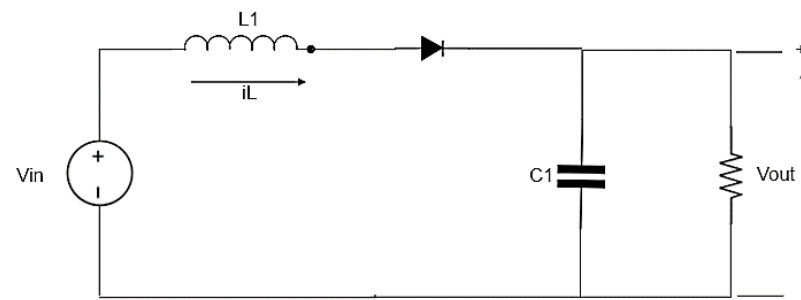


Figure 4. Boost converter.



(a)



(b)

Figure 5. Operation of Boost converter (a) Mode 1, (b) Mode 2.

The waveforms of voltage and current are shown on Figure 6. The selection between continuous conduction mode (CCM) and discontinuous conduction mode (DCM) depends upon factors including input voltage, output voltage, load current, and circuit parameters [40]. The interactions between the inductor’s voltage and current waveforms and other converter components, such as the diode and output capacitor, play an important role in achieving both regulated output voltage and efficient energy transfer. The inductor within a conventional boost converter helps to accumulate and discharge energy to attain the desired output voltage. The inductor’s current waveform undergoes phases of linear increase and decrease, while the inductor’s voltage waveform is contingent upon the input voltage and characteristics of circuit components. The decision between continuous and discontinuous conduction modes substantially influences the behavior of inductor current throughout the switching cycle.

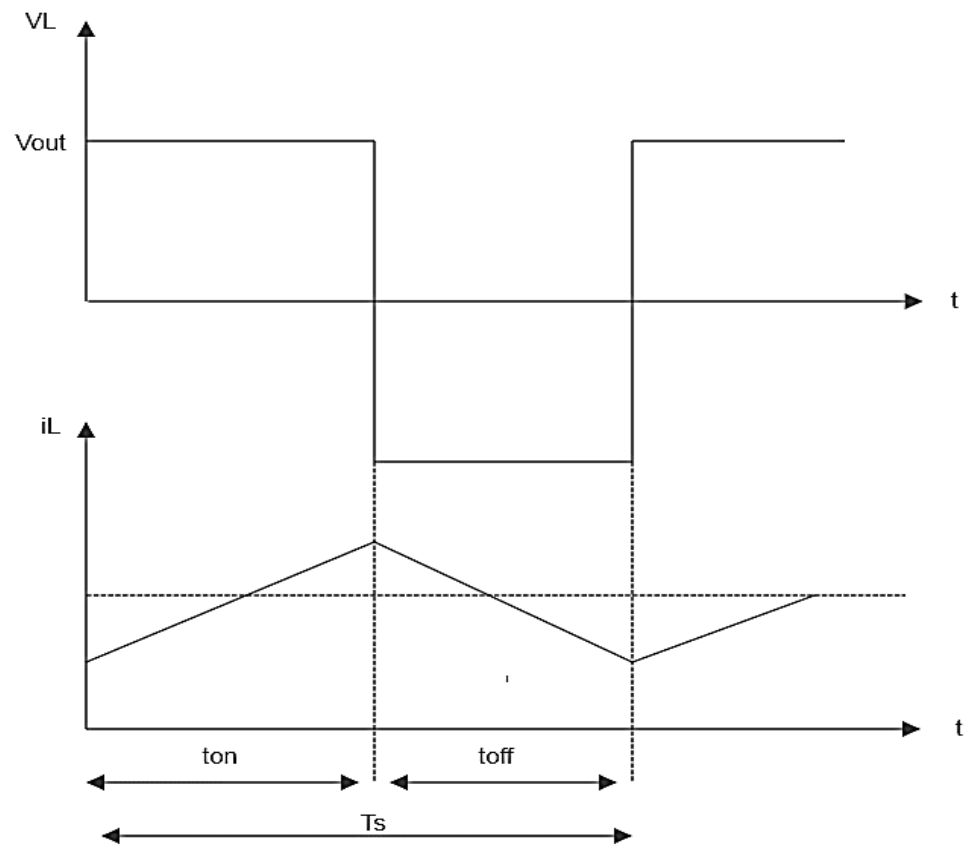


Figure 6. Waveform of output voltage and current.

The output voltage with neglecting the voltage drops across the diode and the transistor is:

$$v_{out} = \frac{V_{in}}{1 - D} \tag{9}$$

### 2.3. Analysis of Proposed Maximum Power Point Tracking Algorithms

#### 2.3.1. P&O-MPPT

P&O algorithm is based on measuring the voltage and current at the output of the PV system to determine the output power. By comparing the new measurements with the previous ones, the algorithm calculates the difference in power and voltage. In the ideal maximum operating point, the change in power ( $\Delta P_{pv}$ ) is zero. However, if  $\Delta P_{pv}$  is not zero, the algorithm adjusts the voltage with a fixed step size to search for the optimal solution. If the PV operating point is on the left side, the algorithm navigates the system towards the right side in the neighborhood of the MPP, and vice versa. This tracking process allows

the P&O algorithm to continuously search for and approach the MPP for efficient power generation [41].

### 2.3.2. INC-MPPT

INC calculates the voltage and current values from the PV system output and determines the derivative of current with respect to voltage considering the instantaneous current-voltage relationship of the PV array [41]. This method tracks the MPP by adjusting the reference voltage based on the system’s operating point. To achieve the MPP, certain conditions must be met:

$$\frac{dP_{pv}}{dV_{pv}} = 0 \tag{10}$$

$$\frac{dP_{pv}}{dV_{pv}} = \frac{I_{pv}dV_{pv}}{dV_{pv}} + \frac{V_{pv}dI_{pv}}{dV_{pv}} \tag{11}$$

and

$$\frac{dI_{pv}}{dV_{pv}} = -I_{pv}/V_{pv} \tag{12}$$

The algorithm increases the reference voltage based on a fixed step voltage when,

$$\frac{dI_{pv}}{dV_{pv}} > 0 \tag{13}$$

While it decreases the reference voltage using the fixed step voltage when

$$\frac{dI_{pv}}{dV_{pv}} < 0 \tag{14}$$

### 2.3.3. PSO-MPPT

PSO exhibits fast convergence, quickly adapting to changes in environmental conditions, and allowing the system to operate close to MPP in a timely manner [42]. Moreover, the simplicity and ease of implementation and robustness in handling noisy or fluctuating conditions marks this approach out, and it can be combined with other optimization techniques or control strategies [43,44]. These factors contribute to the effectiveness and widespread use of PSO in optimizing power extraction from PV systems. The PSO algorithm is as follows:

The Position vector is given in Equation (15).

$$X = [X1, X2, \dots, Xn] \tag{15}$$

The Velocity vector is given in Equation (15)

$$V = [V1, V2, \dots, Vn] \tag{16}$$

Particle’s best position and Global best position are given in Equations (17) and (18) respectively.

$$Pbest = [Pbest1, Pbest2, \dots, Pbestn] \tag{17}$$

$$Gbest = [Gbest1, Gbest2, \dots, Gbestn] \tag{18}$$

The update equation is given in Equation (19).

$$V_{new} = w * V + c1 * rand() * (Pbest - X) + c2 * rand() * (Gbest - X) \tag{19}$$

The position update as

$$X_{new} = X + V_{new} \tag{20}$$

### 2.3.4. GA-MPPT

To analyze the performance of the GA-based MPPT algorithm, it adjusts the algorithm parameters (population Size, and mutation Rate) and observes the best solution and fitness value obtained after the iterations. The initial parent population, denoted as array  $A$ , is initialized to start the optimization process. It consists of individual parent solutions represented by  $X_i = [\text{parent } 1, \text{parent } 2, \dots, \text{parent } n]$ , where  $n$  represents the population size. Each parent solution, parent  $i$  where  $(i = 1, 2, \dots, n)$ , corresponds to the initial voltage values at the beginning of the algorithm. The objective function,  $f(X_i)$ , is used to calculate the output power of the PV system. The fitness values for each position in the population are evaluated based on this objective function [45]. These fitness values are essential for evolving the population and improving the overall fitness of the individuals over successive generations. The GA-MPPT conditions for the PV voltage and power are given as:

$$|V(k + 1) - V(k)| < dV \tag{21}$$

$$|P(k + 1) - P(k)| < dP \tag{22}$$

### 3. Simulation Results and Discussion

The simulation figures depict the verification of the proposed switched capacitor configuration. Figure 7 shows the PV characteristics of the SunPower SPR-440NE-WHT-D, while Figure 8 shows the current vs. voltage and power vs. voltage characteristics for one module. The number of parallel strings ( $N_p$ ) is seven and series connected modules per string ( $N_s$ ) is six for the conventional boost converter (the total number of PV panels is 42). On the other hand, the number of parallel strings is three and series connected modules per string is three for the switched capacitor boost converter (the total number of PV panels is 9). The irradiance and temperature are maintained at a constant as  $100 \text{ W/m}^2$  and  $25 \text{ }^\circ\text{C}$ , respectively. The complete MATLAB/Simulink for the conventional boost converter and the proposed switched capacitor (Fibonacci) is shown in Figure 9.

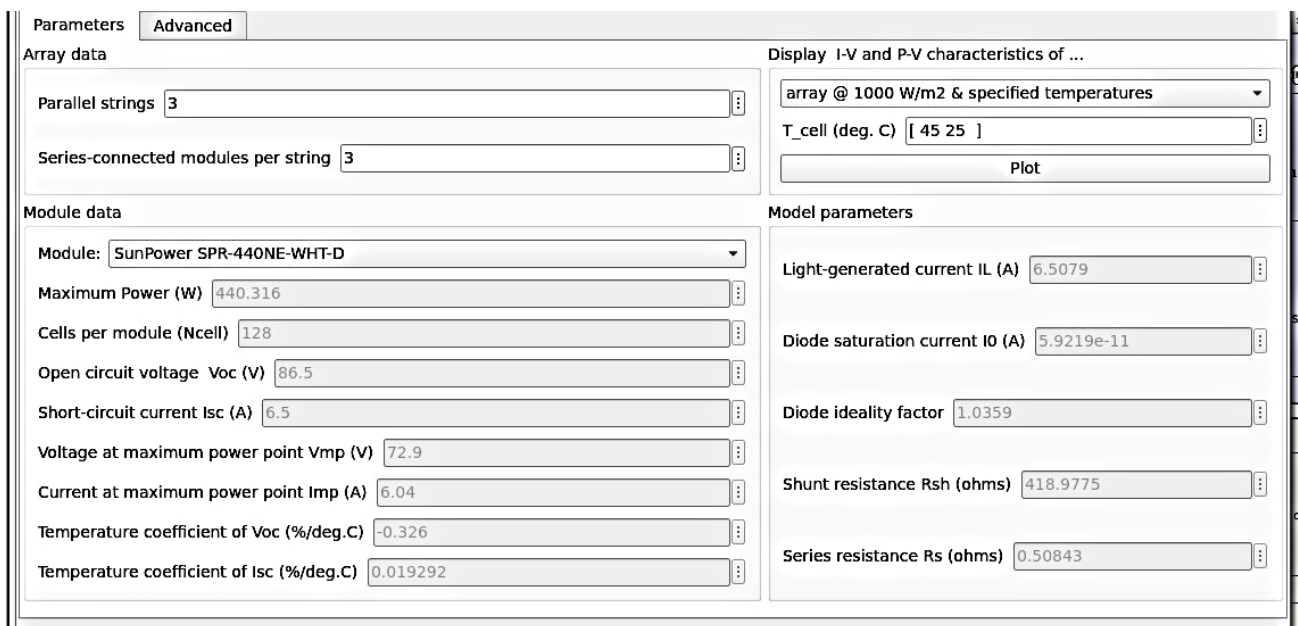


Figure 7. MATLAB/Toolbox PV panel specifications.

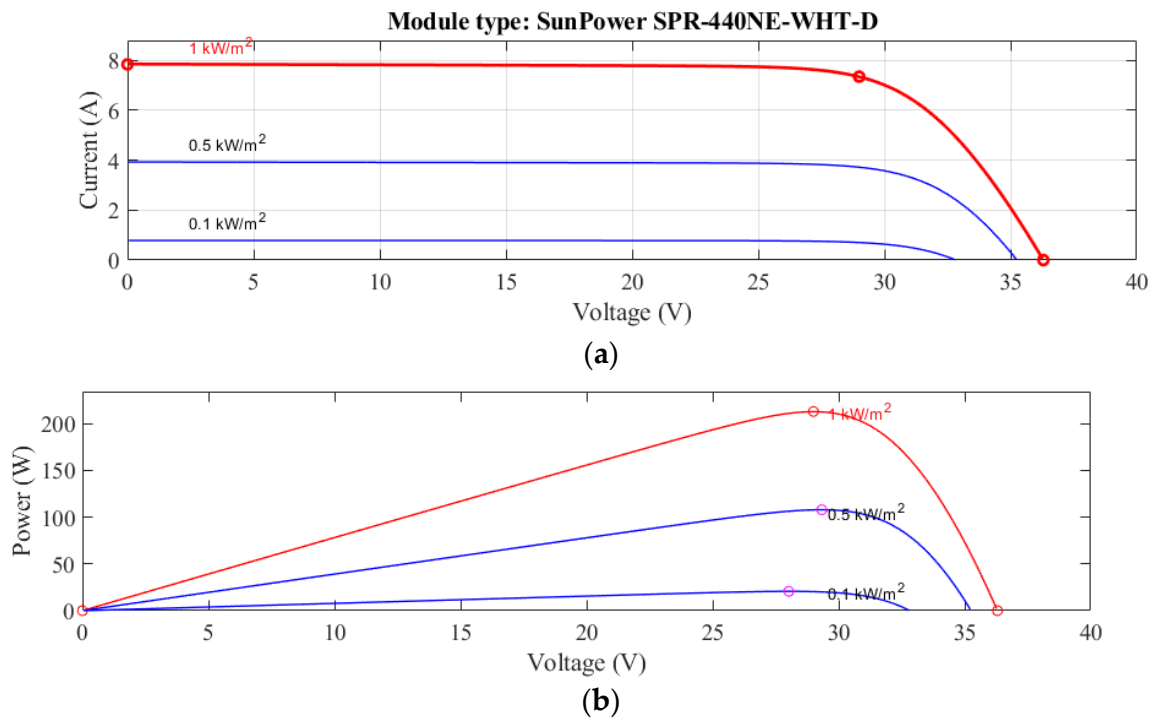


Figure 8. PV solar (a) I-V and (b) P-V characteristics.

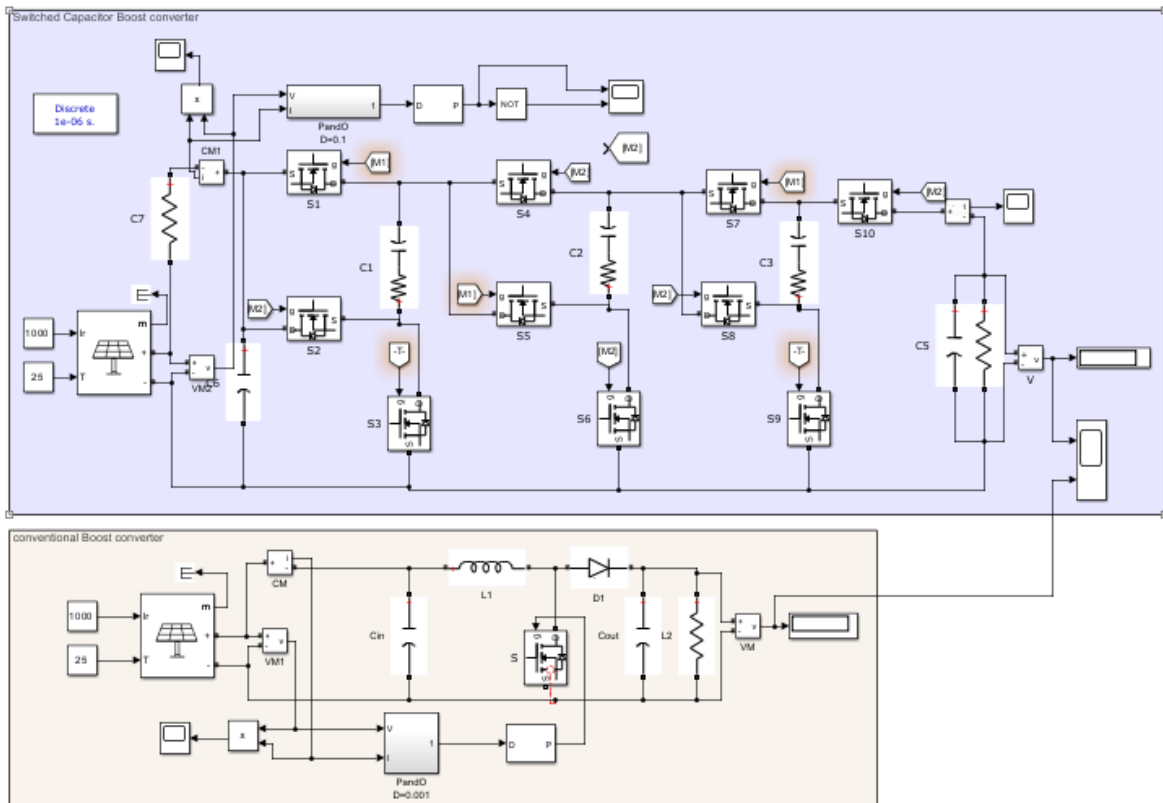


Figure 9. MATLAB/Simulink block diagrams for switched capacitor boost converter and conventional boost converter.

Figure 9 depicts the MATLAB/Simulink block diagram for the two boost configurations, and the conventional and the switched capacitor Fibonacci boost converter. The

values of the system parameters are tabulated in Table 2. This table includes the whole parameters for the two boost converter configurations and for all MPP technologies.

**Table 2.** System Parameters.

Symbol	Definition	Value
PV solar (switched capacitor Boost)		
$N_p$	parallel strings	3
$N_s$	series connected modules per string	3
C1, C2, C3, C4, C5	capacitors	20 $\mu$ F
C6	capacitor	100 $\mu$ F
R1	Input resistance	0.1 $\Omega$
$R_L$	Load resistance	130 $\Omega$
PV solar (conventional Boost)		
$N_p$	parallel strings	7
$N_s$	series connected modules per string	6
Cin, Cout	capacitors	1000, 100 $\mu$ F
$L_1$	inductance	0.9 mH
$R_L$	Load resistance	50 $\Omega$
PSO parameters (for switched capacitor boost converter)		
w	weight	0.79
c1	constant	1.725
c2	constant	1.725
PSO parameters (for conventional boost converter)		
w	weight	0.7
c1	constant	1.025
c2	constant	1.025
GA parameters (for switched capacitor boost converter)		
Population Size	constant	50
Mutation Rate	constant	0.01
GA parameters (for conventional boost converter)		
Population Size	constant	100
Mutation Rate	constant	0.001

In this paper, there are some factors taken into consideration to implement the boost converter with solar PV source. The desired output voltage is defined with respect to the load application, and it is maintained at a constant. These values are dependent on the converter parameters values. However, the input voltage is inconsistent during the comparison. The output voltage of the two boost configurations is compared regarding accuracy, stability, and regulation. Though the voltage ripple, the settling time of the voltage performance has been addressed in the comparison.

In the other hand, the comparison also addresses the output current handling capability of the two boost configurations. It is important to consider that the expected required load current is typically lower than the input current, owing to power conservation principles in boost converters. However, it is worth noting that if the load current is higher than the converter current capability, a voltage drop or damage to the converter will occur. This poses a challenge in designing a converter that can adequately meet the load requirements of a microgrid.

The P&O algorithm is commonly used in small scale industrial applications since it does not require the system characteristics. However, it fails to obtain optimal power from the renewable energy resources.

The output voltage for both the conventional boost converter ( $V_{con}$ ) and the switched capacitor boost converter ( $V_{sc}$ ) are shown in Figure 4. The output voltage is settled down at 0.2 s for the conventional boost converter, while for the switched capacitor boost the settling time is less than 0.08 s when the P&O MPPT is used. Figure 10 illustrates the output voltage and output current for both conventional boost converter and the switched capacitor boost

converter under the P&O MPPT algorithm. The improved overshoot characteristics of a capacitor-switched boost converter can be attributed to the inherent properties of its operation. Figures 11–13 show the output voltage under the various MPPT algorithms. The system parameters are tabulated in Table 2.

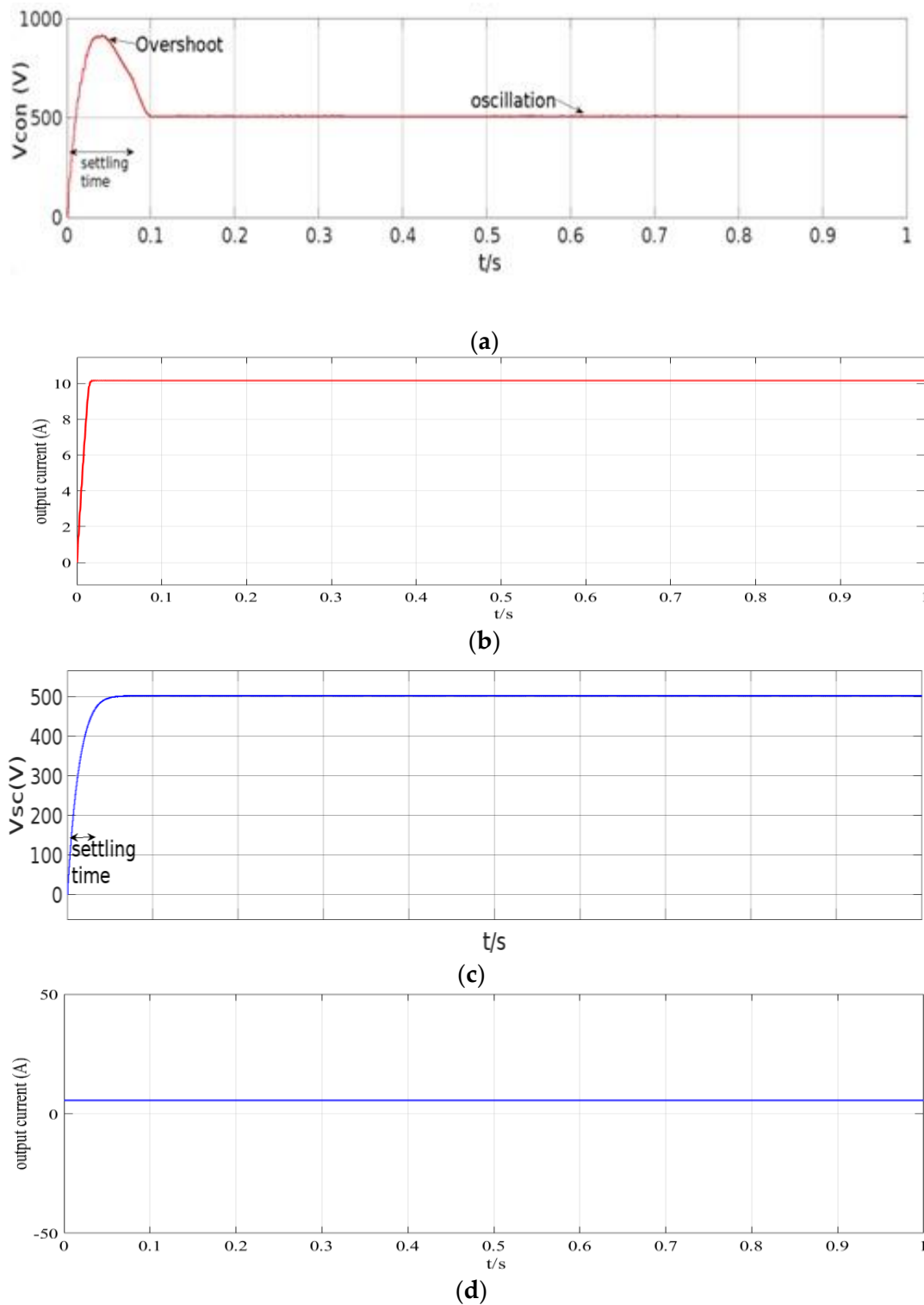
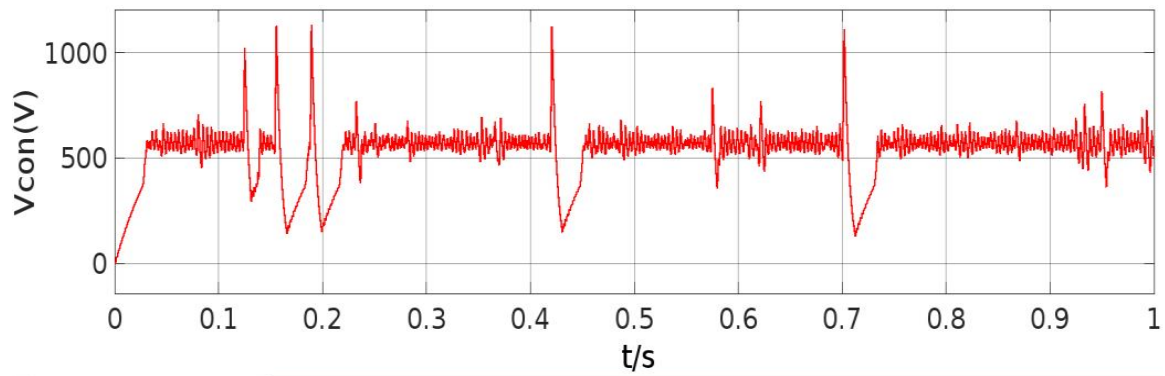
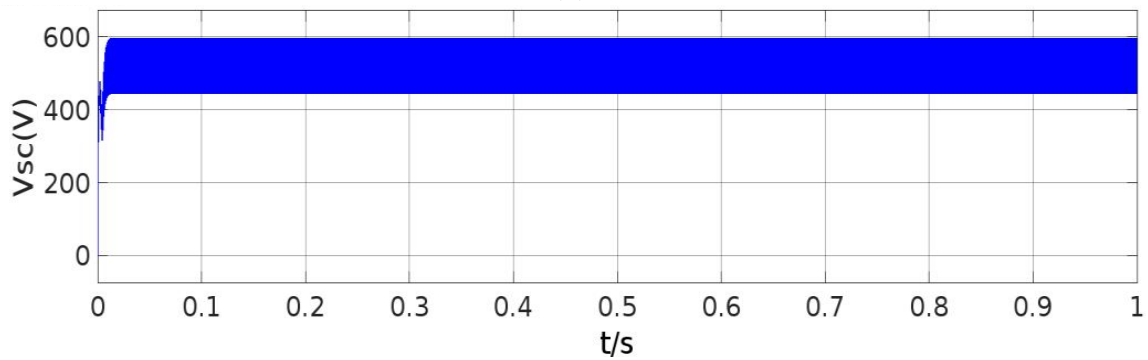


**Figure 10.** P&O MPPT simulation results for: conventional boost converter (a) output voltage, (b) output current, and switched capacitor boost converter (c) output voltage, (d) output current.

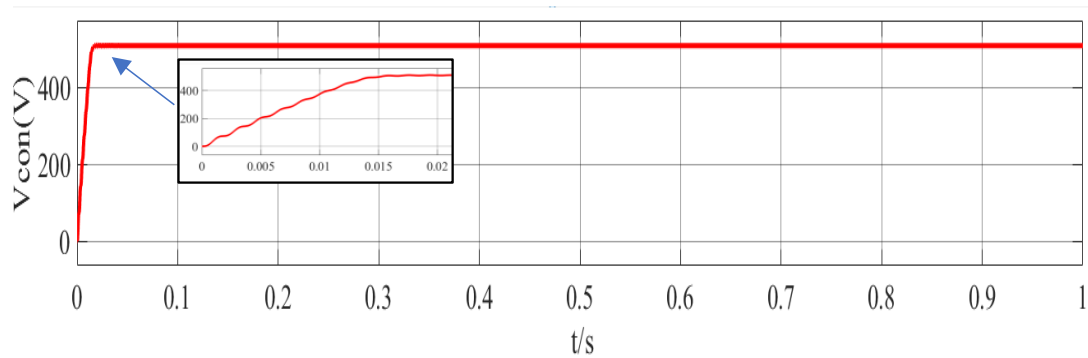


(a)

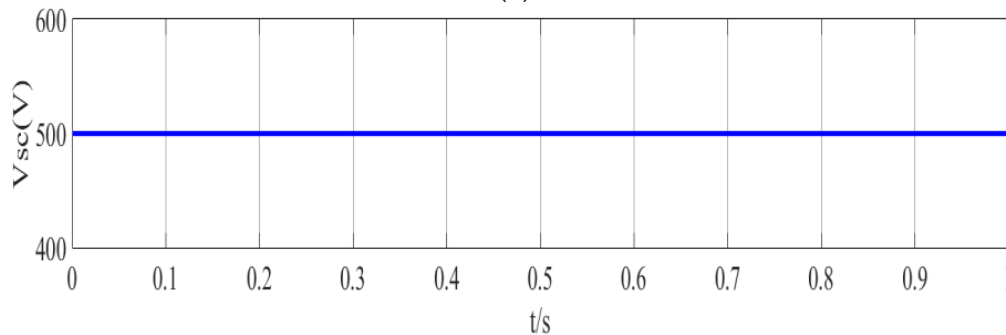


(b)

**Figure 11.** Output voltage using INC MPPT for (a) conventional boost converter ( $V_{con}$ ) and (b) switched capacitor boost converter ( $V_{sc}$ ).



(a)



(b)

**Figure 12.** Output voltage using PSO MPPT for (a) conventional boost converter ( $V_{con}$ ) and (b) switched capacitor boost converter ( $V_{sc}$ ).

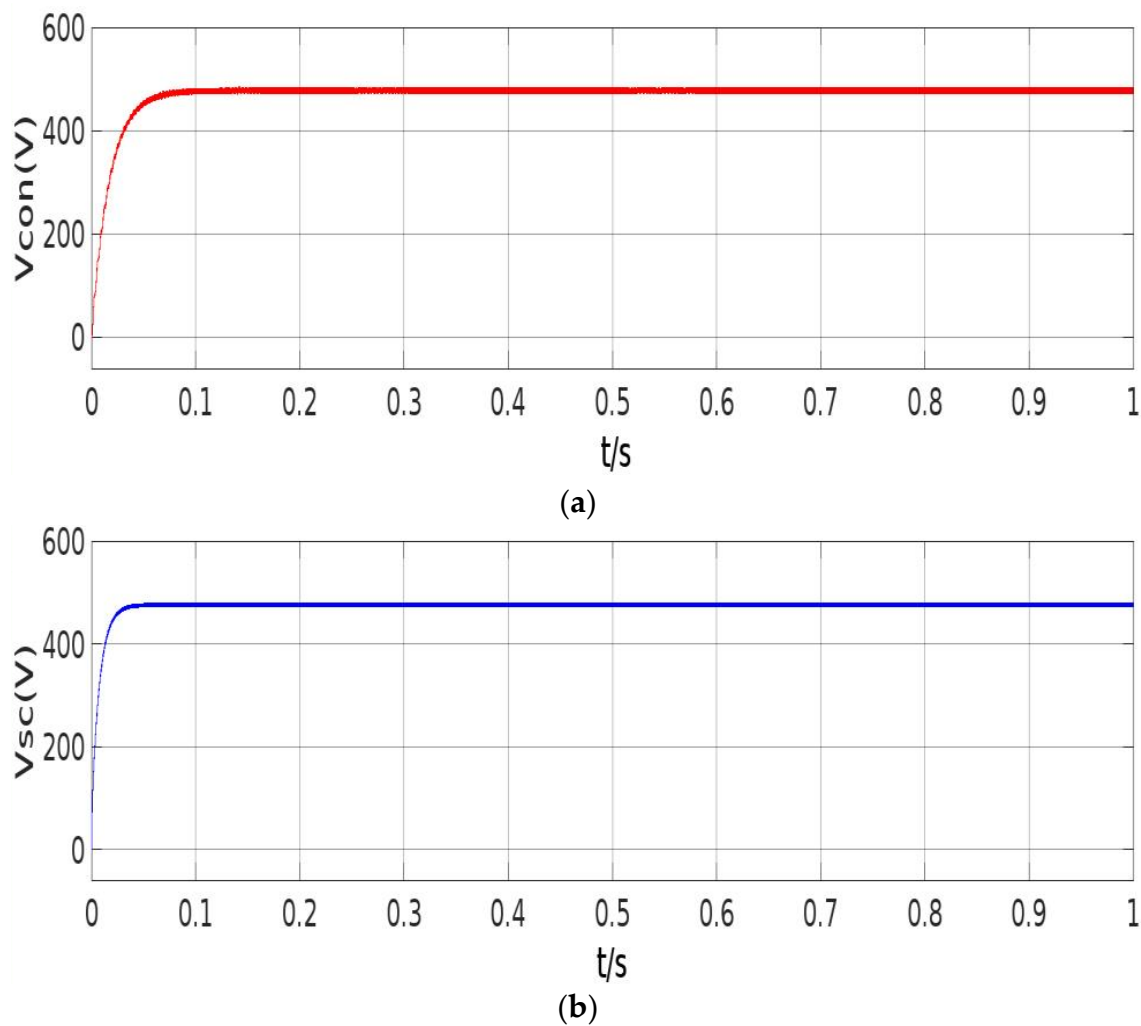


**Figure 13.** Output voltage using GA MPPT for (a) conventional boost converter and (b) ( $V_{con}$ ) switched capacitor boost converter ( $V_{sc}$ ).

The simulation results in Figure 10 demonstrate that the output current capability of the conventional boost converter is higher than that of the switched capacitor boost converter. The selection of the appropriate boost converter type should be made based on a thorough assessment of the application’s requirements, including voltage and current levels, efficiency, transient response, and overall system design constraints.

The switched capacitor Boost converter utilizes capacitors ( $C_1$ ,  $C_2$ ,  $C_3$ ,  $C_4$ ,  $C_5$ , and  $C_6$ ) to achieve voltage boosting, while the conventional Boost converter uses inductance ( $L_1$ ) in addition to capacitors ( $C_{in}$  and  $C_{out}$ ) for voltage boosting. The switched capacitor Fibonacci boost converter employs capacitors ( $C_1$  to  $C_6$ ) with values of  $20 \mu\text{F}$  and  $100 \mu\text{F}$ , while the conventional boost converter uses capacitors ( $C_{in}$  and  $C_{out}$ ) with values of  $1000 \mu\text{F}$  and  $100 \mu\text{F}$ , respectively.

The simulation results in Table 3 shows that the switched capacitor boost converter plays an important role in enhancing the MPPT performance. Since the switched capacitor smooths the output voltage and maintains a stable voltage, the conventional converter smooths the current fluctuations. In addition, the GA-MPPT algorithm based on switched capacitor boost converter provides better MPP tracking performance compared with the other MPPT algorithms. The current capability values for each converter based on GA-MPPT are given in Table 3. The switched capacitor has a significantly greater current than that of the conventional converter. According to the values of the current capability, the switches are designed and expected to handle high power applications requirements.

Consequently, the comparison between conventional and switched capacitor Fibonacci boost configurations for MPPT methods reveals significant advantages for the switched capacitor configuration. With significantly faster settling times, ranging from less than 1 ms to 0.008 s, and lower output oscillation percentages of 0.02% to 1.02%, the switched capacitor boost configuration outperforms its conventional counterpart across different MPPT methods. This suggests that the switched capacitor Fibonacci boost configuration offers improved performance, stability, and efficiency for maximizing power output in PV solar systems compared to the conventional boost configuration.

**Table 3.** Simulation results comparison based on the performance of the output voltage.

Boost Configuration Type	MPPT Method	Settling Time (s)	Output Oscillation %
Conventional	P&O	0.2	0.5
Switched capacitor		0.008	0.02
Conventional	INC	0.05	70
Switched capacitor		0.008	25
Conventional	PSO	0.02	0.8
Switched capacitor		<1 ms	1.02
Conventional	GA	0.04	0.5
Switched capacitor		0.03	0.02

The analysis is extended by including additional evaluation data or comparing the GA-based MPPT algorithm with other MPPT techniques. The simulation results for current capability comparison based on the GA-MPPT reveal significant differences between the conventional and switched capacitor Fibonacci boost configurations. The conditions of the GA-based MPPT technique ensure that it adapts to sudden variations in load and solar irradiance, allowing it to effectively optimize the MPPT process over time.

The conventional boost configuration achieves a maximum output current of 10 A; the switched capacitor Fibonacci boost configuration significantly outperforms it, with a maximum output current of 70 A. This indicates that the switched capacitor boost configuration demonstrates a substantially higher current capability, making it more suitable for applications that require greater power output and current handling capacity, see Table 4.

**Table 4.** Current capability simulation results comparison based on the GA-MPPT.

Boost Configuration Type	Maximum Output Current (A)
Conventional	10
Switched capacitor	70

In conclusion, for the P&O-MPPT method, the conventional boost configuration exhibits a settling time of 0.2 s with an output oscillation of 0.5%. In contrast, the switched capacitor boost configuration demonstrates a significantly improved performance with a settling time of 0.008 s an output oscillation of 0.02%.

When considering the INC-MPPT method, the conventional boost configuration has a settling time of 0.05 s, with a high output oscillation of 70%. Conversely, the switched capacitor boost configuration displays a superior performance, with a settling time of 0.008 s and a reduced output oscillation of 25%.

For the PSO-MPPT method, the conventional boost configuration achieves a settling time of 0.02 s, with an output oscillation of 0.8%. The switched capacitor boost configuration showcases exceptional speed with a settling time of less than 1 msec and a slightly increased output oscillation of 1.02%.

Under the GA-MPPT method, the conventional boost configuration demonstrates a settling time of 0.04 s with an output oscillation of 0.5%. The switched capacitor boost

configuration offers a comparable settling time of 0.03 s and an even lower output oscillation of 0.02%.

Moreover, when examining the current capability simulations based on the GA-MPPT, the conventional boost configuration achieves a maximum output current of 10 A. In contrast, the switched capacitor boost configuration significantly outperforms it, delivering a maximum output current of 70 A.

The switched capacitor configuration demonstrates faster settling times, lower output oscillations, and significantly higher current capability, making it a more promising option for maximizing power output and achieving efficient MPPT in PV solar systems.

Moreover, GA effectively mitigated the negative effects of P&O, INC, and metaheuristic PSO. The GA-MPPT algorithm does not experience any transient oscillations observed in PSO or the steady-state oscillation effects encountered by P&O. Additionally, the GA demonstrates superior robustness compared to other tracking algorithms, particularly in handling inferior regions of the MPP.

#### 4. Conclusions

This paper examined and compared the performance of two boost converter topologies, conventional and switched capacitor integrated with MP harvest from the solar PV source. In addition, four MPPT algorithms (P&O, INC, PSO, and GA) were implemented to enhance the tracking power for each boost converter. The simulation results showed that the conventional boost converter provides suitable current handling capability. On the other hand, the switched capacitor boost converter demonstrates good voltage step up performance. Furthermore, the various MPPT algorithms are utilized in enhancing the converter MPP tracking performance. The P&O and INC algorithms offer simplicity and ease of implementation, while the GA and PSO algorithms required optimization setup. It can be concluded that the switched capacitor exhibits suitable performance in terms of output voltage performance and current capability when integrated with MPPT. The GA and PSO algorithms achieve better maximum power accuracy. The switched capacitor boost converter consistently demonstrates improved performance in terms of rising time, overshoot, and oscillation across multiple MPPT algorithms. Future work could involve further optimization techniques to enhance system reliability and accuracy in tracking multiple power peaks and achieving faster MPP attainment.

**Author Contributions:** Conceptualization, M.H. and M.A.Z.; methodology, M.H. and H.M.D.H.; software, and validation, formal analysis, E.A.; investigation; resources, M.H. and M.Y., data curation, writing, M.H. and H.M.D.H.; writing and design verification, M.A.Z.; supervision, project administration, funding acquisition, M.H. All authors have read and agreed to the published version of the manuscript.

**Funding:** This research received no external funding.

**Conflicts of Interest:** The authors declare no conflict of interest.

#### Abbreviations

BA	Bat algorithm
DE	Differential Evaluation
EMI	Electromagnetic interference
FSSC	Fibonacci Sequence Switched Capacitor converter
FSSC	Fibonacci Sequence Switched Capacitor converter
GA	Genetic Algorithm
INC	Increment Conductance
MPPT	Maximum Power Point Tracking
P&O	Perturb & Observe
PSO	Particle Swarm Optimization
SCBC	Switch Capacitor Boost Converter
SMPS	Switched-Mode Power Supply

## References

1. Qian, T.; Yang, Y.; Zhao, W. A Boost-Type Three-Port Resonant Forward Converter with Flexible Power Flow Path Optimization for PV Systems. *IEEE Trans. Circuits Syst. II Express Briefs* **2023**, *70*, 161–165. [CrossRef]
2. Yoon, D.; Cho, Y.; Bae, S.; Lee, J. An Input-Series Output-Series Noninverting Buck–Boost Converter for 1500 V DC Bus with Wide Input and Output Voltage Ranges. *IEEE Trans. Ind. Electron.* **2023**, *70*, 11231–11241. [CrossRef]
3. Mouselinos, T.P.; Tatakis, E.C. Investigation of Highly Efficient Five Level Asymmetrical Inverter Family with Embedded Buck–Boost Converter. *IEEE Access* **2022**, *10*, 88750–88768. [CrossRef]
4. Saafan, A.A.; Khadkikar, V.; El Moursi, M.S.; Zeineldin, H.H. A New Multiport DC–DC Converter for DC Microgrid Applications. *IEEE Trans. Ind. Appl.* **2023**, *59*, 601–611. [CrossRef]
5. Li, B.; Zhang, B.; Zhang, Y.; Li, L.; Xu, D. Design and Implementation of a High-Power DC/DC Converter for HVDC Interconnections with Wide DC Voltage Range and Fault-Blocking Capability. *IEEE J. Emerg. Sel. Top. Power Electron.* **2022**, *10*, 785–799. [CrossRef]
6. Khan, M.S.; Nag, S.S.; Das, A.; Yoon, C. Analysis and Control of an Input-Parallel Output-Series Connected Buck–Boost DC–DC Converter for Electric Vehicle Powertrains. *IEEE Trans. Transp. Electrification* **2023**, *9*, 2015–2025. [CrossRef]
7. Alhawsawi, E.Y.; Habbi, H.M.D.; Hawsawi, M.; Zohdy, M.A. Optimal Design and Operation of Hybrid Renewable Energy Systems for Oakland University. *Energies* **2023**, *16*, 5830. [CrossRef]
8. Chappell, P.H. Introduction to power electronics. In *Artech House Power Engineering Library*; Artech House: Boston, UK; Massachusetts, UK, 2013.
9. Law, K.; Cheng, K.; Yeung, Y. Design and analysis of switched-capacitor-based step-up resonant converters. *IEEE Trans. Circuits Syst. I Regul. Pap.* **2005**, *52*, 943–948. [CrossRef]
10. Rashid, M.H. *Power Electronics Handbook*; Elsevier Science & Technology: Saint Louis, MS, USA, 2017. Available online: <http://ebookcentral.proquest.com/lib/oakland/detail.action?docID=5043418> (accessed on 16 June 2023).
11. Xue, W.; Zhang, Y.; Lu, Y.; Fang, J.; Ren, J. A Two-Phase Hybrid Switched Capacitors Converter with Interleaving Control Scheme for Flying Capacitors Self-Balancing. In Proceedings of the 2023 IEEE Applied Power Electronics Conference and Exposition (APEC), Orlando, FL, USA, 19–23 March 2023; pp. 2111–2115. [CrossRef]
12. Sagpazar, N.B.; Cho, W.; Kim, K.; Choi, S. Three-level Resonant Switched Capacitor Boost Converter. In Proceedings of the 2019 10th International Conference on Power Electronics and ECCE Asia (ICPE 2019—ECCE Asia), Busan, Republic of Korea, 27–30 May 2019; pp. 2868–2873. [CrossRef]
13. Evzelman, M.; Ben-Yaakov, S. The effect of switching transitions on switched capacitor converters losses. In Proceedings of the 2012 IEEE 27th Convention of Electrical and Electronics Engineers in Israel, Eilat, Israel, 14–17 November 2012; pp. 1–5. [CrossRef]
14. Zhu, J. Transformerless Stacked Active Bridge DC–DC Converters: Analysis, Synthesis and Design. Ph.D. Thesis, University of Colorado at Boulder, Boulder, CO, USA, 2020. Available online: <https://www.proquest.com/dissertations-theses/transformerless-stacked-active-bridge-dc/docview/2474854084/se-2?accountid=12924> (accessed on 26 July 2023).
15. Thota, P.R.; Jeevananthan, S. A New Switched Capacitor Nine-Level Inverter with Quadruple Voltage Boosting and Capacitor Voltage Balancing Capabilities. In Proceedings of the 2020 IEEE International Conference on Power Electronics, Drives and Energy Systems (PEDES), Jaipur, India, 16–19 December 2020; pp. 1–5.
16. SinghNeti, S.; Singh, V. A Reduce Device Count Nine Level MLI Using Switched Capacitors. In Proceedings of the 2020 First International Conference on Power, Control and Computing Technologies (ICPC2T), Raipur, India, 3–5 January 2020; pp. 210–214. [CrossRef]
17. Khorasani, R.R.; Jazi, H.M.; Chaudhuri, N.R.; Khoshkbar-Sadigh, A.; Shaneh, M.; Adib, E.; Wheeler, P. An Interleaved Soft Switched High Step-Up Boost Converter with High Power Density for Renewable Energy Applications. *IEEE Trans. Power Electron.* **2022**, *37*, 13782–13798. [CrossRef]
18. Mondal, S.; Biswas, S.P.; Islam, R.; Muyeen, S.M. A Five-Level Switched-Capacitor Based Transformerless Inverter with Boosting Capability for Grid-Tied PV Applications. *IEEE Access* **2023**, *11*, 12426–12443. [CrossRef]
19. Ali, M.; Tayyab, M.; Sarwar, A.; Khalid, M. A Low Switch Count 13-Level Switched-Capacitor Inverter with Hexad Voltage-Boosting for Renewable Energy Integration. *IEEE Access* **2023**, *11*, 36300–36308. [CrossRef]
20. Rahimi, R.; Habibi, S.; Shamsi, P.; Ferdowsi, M. A Three-Winding Coupled-Inductor-Based Dual-Switch High Step-Up DC–DC Converter for Photovoltaic Systems. *IEEE J. Emerg. Sel. Top. Ind. Electron.* **2022**, *3*, 1106–1117. [CrossRef]
21. Khorasani, R.R.; Jazi, H.M.; Khoshkbar-Sadigh, A.; Chaudhuri, N.R.; Shaneh, M.; Nourieh, N.; Adib, E.; Wheeler, P. ZVT High Step-Up Boost Converter With Wide Input Voltage and Wide Output Power for Renewable Energy Applications. *IEEE J. Emerg. Sel. Top. Power Electron.* **2022**, *10*, 6057–6069. [CrossRef]
22. Zheng, L.; Kandula, R.P.; Divan, D. Soft-Switching Solid-State Transformer with Reduced Conduction Loss. *IEEE Trans. Power Electron.* **2021**, *36*, 5236–5249. [CrossRef]
23. Murtaza, A.F.; Sher, H.A.; Khan, F.U.; Nasir, A.; Spertino, F. Efficient MPP Tracking of Photovoltaic (PV) Array Through Modified Boost Converter with Simple SMC Voltage Regulator. *IEEE Trans. Sustain. Energy* **2022**, *13*, 1790–1801. [CrossRef]
24. Murtaza, A.F.; Sher, H.A. A Series Resonant Network based Boost Converter. In Proceedings of the 2023 International Conference on Emerging Power Technologies (ICEPT), Topi, Pakistan, 6–7 May 2023; pp. 1–4. [CrossRef]

25. Lin, H.; Chan, W.C.; Lee, W.K.; Chen, Z.; Chan, M.; Zhang, M. High-Current Drivability Fibonacci Charge Pump With Connect-Point-Shift Enhancement. *IEEE Trans. Very Large Scale Integr. (VLSI) Syst.* **2017**, *25*, 2164–2173. [[CrossRef](#)]
26. Mahnashi, Y.; Peng, F.Z. A Monolithic Voltage-Scalable Fibonacci Switched-Capacitor DC–DC Converter With Intrinsic Parasitic Charge Recycling. *IEEE Trans. Very Large Scale Integr. (VLSI) Syst.* **2019**, *27*, 1105–1113. [[CrossRef](#)]
27. Mahnashi, Y.; Peng, F.Z. Generalization of the Fundamental Limit Theory in a Switched-Capacitor Converter. *IEEE Trans. Power Electron.* **2017**, *32*, 6673–6676. [[CrossRef](#)]
28. Makowski, M. Realizability conditions and bounds on synthesis of switched-capacitor DC-DC voltage multiplier circuits. *IEEE Trans. Circuits Syst. I Regul. Pap.* **1997**, *44*, 684–691. [[CrossRef](#)]
29. Mahnashi, Y. A New Approach to Improve the Voltage Conversion Ratio in Topological Switched-Capacitor DC–DC Converters Using Negator Stage. *IEEE Trans. Circuits Syst. II Express Briefs* **2023**, *70*, 1465–1469. [[CrossRef](#)]
30. Uno, M.; Igarashi, R.; Sato, Y. Switched Capacitor-Based PWM- and Phase Shift-Controlled Multiport Converter With Differential Power Processing Capability for Standalone Photovoltaic Systems Under Partial Shading. *IEEE J. Emerg. Sel. Top. Power Electron.* **2021**, *9*, 6019–6032. [[CrossRef](#)]
31. Farsi, M.; Liu, J. An Application to Solar Photovoltaic Systems. In *Model-Based Reinforcement Learning: From Data to Continuous Actions with a Python-Based Toolbox*; IEEE: Hoboken, NJ, USA, 2023; pp. 147–185. [[CrossRef](#)]
32. Deboucha, H.; Shams, I.; Belaid, S.L.; Mekhilef, S. A Fast GMPPT Scheme Based on Collaborative Swarm Algorithm for Partially Shaded Photovoltaic System. *IEEE J. Emerg. Sel. Top. Power Electron.* **2021**, *9*, 5571–5580. [[CrossRef](#)]
33. Kacimi, N.; Idir, A.; Grouni, S.; Boucherit, M.S. Improved MPPT Control Strategy for PV Connected to Grid Using IncCond-PSO-MPC Approach. *CSEE J. Power Energy Syst.* **2023**, *9*, 1008–1020. [[CrossRef](#)]
34. Elgharib, A.O.; Alhasheem, M.; Swief, R.A.; Naamane, A. Wind Turbine Performance Assessment Boost Converter Based Applying PI Controller Integrating Genetic Algorithm. In Proceedings of the 2021 International Conference on Microelectronics (ICM), New Cairo City, Egypt, 19–22 December 2021; pp. 236–241. [[CrossRef](#)]
35. Joisher, M.; Singh, D.; Taheri, S.; Espinoza-Trejo, D.R.; Pouresmaeil, E.; Taheri, H. A Hybrid Evolutionary-Based MPPT for Photovoltaic Systems Under Partial Shading Conditions. *IEEE Access* **2020**, *8*, 38481–38492. [[CrossRef](#)]
36. Eltamaly, A.M.; Al-Saud, M.S.; Abokhalil, A.G. A Novel Bat Algorithm Strategy for Maximum Power Point Tracker of Photovoltaic Energy Systems Under Dynamic Partial Shading. *IEEE Access* **2020**, *8*, 10048–10060. [[CrossRef](#)]
37. Murtaza, A.F.; Sher, H.A.; Chiaberge, M.; Boero, D.; De Giuseppe, M.; E Addoweesh, K. Optimization of the perturb and observe maximum power point tracker for a distributed photovoltaic system. In Proceedings of the INMIC, Lahore, Pakistan, 19–20 December 2013; pp. 77–82. [[CrossRef](#)]
38. de Souza, A.F.; Tofoli, F.L.; Ribeiro, E.R. Switched Capacitor DC-DC Converters: A Survey on the Main Topologies, Design Characteristics, and Applications. *Energies* **2021**, *14*, 2231. [[CrossRef](#)]
39. Chan, C.-Y. A Nonlinear Control for DC–DC Power Converters. *IEEE Trans. Power Electron.* **2007**, *22*, 216–222. [[CrossRef](#)]
40. Banerjee, S.; Ghosh, A.; Padmanaban, S. Modeling and analysis of complex dynamics for dSPACE controlled closed-loop DC-DC boost converter. *Int. Trans. Electr. Energy Syst.* **2019**, *29*, e2813. [[CrossRef](#)]
41. Ibrahim, M.H.; Ang, S.P.; Dani, M.N.; Rahman, M.I.; Petra, R.; Sulthan, S.M. Optimizing Step-Size of Perturb & Observe and Incremental Conductance MPPT Techniques Using PSO for Grid-Tied PV System. *IEEE Access* **2023**, *11*, 13079–13090. [[CrossRef](#)]
42. Ishaque, K.; Salam, Z.; Amjad, M.; Mekhilef, S. An Improved Particle Swarm Optimization (PSO)-Based MPPT for PV With Reduced Steady-State Oscillation. *IEEE Trans. Power Electron.* **2012**, *27*, 3627–3638. [[CrossRef](#)]
43. Habbi, H.M.; Alhamadani, A. Implementation of Power System Stabilizer Based on Conventional and Fuzzy Logic Controllers. *J. Eng.* **2018**, *24*, 97–113. [[CrossRef](#)]
44. Koh, J.S.; Tan, R.H.G.; Lim, W.H.; Tan, N.M.L. A Modified Particle Swarm Optimization for Efficient Maximum Power Point Tracking Under Partial Shading Condition. *IEEE Trans. Sustain. Energy* **2023**, *14*, 1822–1834. [[CrossRef](#)]
45. Yap, K.Y.; Sarimuthu, C.R.; Lim, J.M.-Y. Artificial Intelligence Based MPPT Techniques for Solar Power System: A review. *J. Mod. Power Syst. Clean Energy* **2020**, *8*, 1043–1059. [[CrossRef](#)]

**Disclaimer/Publisher’s Note:** The statements, opinions and data contained in all publications are solely those of the individual author(s) and contributor(s) and not of MDPI and/or the editor(s). MDPI and/or the editor(s) disclaim responsibility for any injury to people or property resulting from any ideas, methods, instructions or products referred to in the content.